Wave Propagation Modeling in Tunnels

Ferenc Lénárt, Budapest University of Technology and Economics,
Department of Broadband Infocommunications and Electromagnetic Theory

Abstract

The new mobile network system design needs more precise characterization of the radio channel and needs sophisticated propagation models, because of the higher data rates. Especially planning coverage in tunnels and indoor spaces causes design problems without these models.

Indoor propagation problems for wideband radio systems are investigated widely and one of the today applied approach of modeling is the special ray-tracing the ray-launching method. These ray methods are efficient for parallel-perpendicular scenarios but there is a common problem tracing the rays for curved surfaces. The other disadvantage of the ray methods is the difficulty in describing the diffraction for a complex scenario. The specific case of the straight circular tunnel can be modeled analytically as a waveguide with circular cross-section.

1. Introduction

In the radio network design practice empirical, semi-empirical and deterministic radio wave propagation methods are used to field strength estimation. The 3-4 generation system designers need broadband characterization of the radio channel and coverage prediction, which is based on any deterministic propagation models. The receiver designers also need precise stochastic description of the radio channel to develop the equalizer and estimation of the receiver. The indoor base station and radio access points are usually used to extend coverage to indoor areas where outdoor signals do not reach well, or to add network capacity in areas with very dense mobile device usage.

The deterministic models generally based on ray tracing or on direct solution of the Maxwell's equations. The first step of the ray tracing methods is solving a pure geometrical problem, but in special cases this leads to very complex analysis especially for curved building geometries, highway and underground tunnels, and for highly reflective building

media, like reinforced concrete. In such cases the trace and store of few million rays results in huge memory requirement and calculation time for multiple reflection, transmission and diffraction. The other disadvantage of the ray methods is the difficulty in describing the diffraction for a complex scenario. In related papers ray tracing method introduced where bundles of rays are used to represent each "physical" wave. Monte Carlo techniques were used for the ray launching. Each bundle of rays was traced to a receiver position where reception spheres determined which rays are intercepted by the receiver.

The Maxwell's equations can be solved directly using parabolic type equations or in differential form using Finite Difference Time Domain (FDTD) method.

2. Wave propagation mechanisms

The effect of difficult and complex geometry of radio wave propagation environment can be simplified to simple physical models as direct, reflected, transmitted and diffracted paths. The ray tracing propagation modeling method first solve the geometrical problem, and after partitioning the wave into rays the simple physical methods above are used to describe the interaction between the propagating waves and materials.

2.1. Direct path

The direct path is to be considered the propagation in Line of Sight (LOS), where the receiver is in direct visibility with the transmitter. In terms of radiowave propagation being in LOS means having the cleared Fresnel zones all along the path.

If the transmitter antenna of gain G_A is fed by P_A input power, than the radiated power density at a distance r assuming LOS spherical wave propagation would be

$$S_o = \frac{P_A G_A}{4\pi r^2} \tag{1}$$

In the far field region of the transmitter antenna the electric and magnetic field strength vectors are mutually perpendicular to each others and of propagation direction, and are in phase. Therefore the power density can be described as

$$S_o = \frac{|\mathbf{E}|^2}{240\pi} \tag{2}$$

The electrical field strength magnitude can be derived from (1) and (2) as

$$E = \frac{\sqrt{60 P_A G_A}}{r} \tag{3}$$

The (3) shows an electrical field strength magnitude change inversely proportional with distance for spherical waves, and the received power squared inversely proportional with distance. For two-dimensional problem, the electrical field strength dependence is $E \approx 1/\sqrt{r}$ in case of cylindrical wave.

2.2. Reflection

Reflection occurs when a propagating electromagnetic wave impinges upon an object which has very large dimensions when compared to the wavelength of the propagating wave. Reflections occur from the surface of the earth and from buildings and walls. The amplitude, phase and polarization of the reflected wave depend on the reflection medium material parameters and the surface irregularity. If the interaction surface plane and perfectly smooth than specular reflection is observed and the energy flow is discrete in space. This ideal case can be modeled using the Snell-Descartes law extended for lossy dielectrics. In most cases for radio wave propagation problems the media are diamagnetic or nonmagnetic so its relative permeability is 1.

The reflection coefficient for plane waves is defined as the complex electric field strength ratio of the incoming and the reflected wave ($R = E_r / E_i$), which is decomposed into its perpendicular and parallel components. (Figure 1)

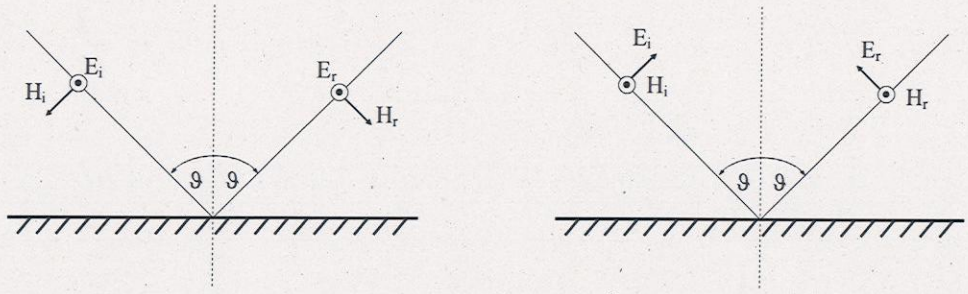

Figure 1 Perpendicular ⊥ (hard or TE) polarization Parallel || (soft or TM) polarization

The reflection coefficient for the two polarization state

$$R_{\perp} = \frac{\cos\vartheta - \sqrt{\varepsilon_r + \cos^2\vartheta - 1}}{\cos\vartheta + \sqrt{\varepsilon_r + \cos^2\vartheta - 1}} \qquad R_{\parallel} = \frac{\varepsilon_r \cos\vartheta - \sqrt{\varepsilon_r + \cos^2\vartheta - 1}}{\varepsilon_r \cos\vartheta + \sqrt{\varepsilon_r + \cos^2\vartheta - 1}} \tag{4}$$

where ε_r is the ratio of the complex dielectric material parameter for the two media on the planar interface.

The Figure 2 shows stationary field excited by a $\perp$ polarized point source in the upper half plane, with sinusoidal time dependence, the reflection material complex permittivity is ε_r = 3-1*j, and the area of investigation is 10λ*15λ. The typical interference picture shows wave front undulation and significant field strength decreasing in several directions.

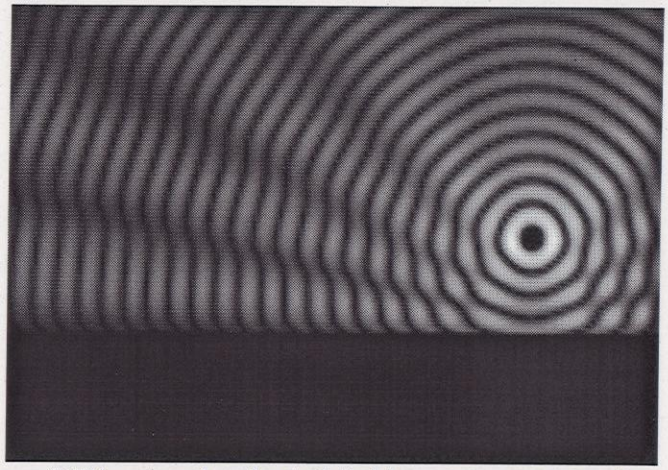

Figure 2 Direct and reflected field component interference

2.3. Transmission

The transmission coefficient (throughput loss) $T = E_t / E_i$ is used to represent the electrical field strength ratio of the electromagnetic incident and transmitted wave at the interface of two media.

General formulation of the reflection and transmission coefficients of multiple material layers can be developed for uniform plane wave at oblique angle incidence using the transmission line theory. The model is based on the well known impedance transfer equation for transmission lines with different characteristic impedance. The results on Figure 3 are presenting the simulated transmission coefficients as a function of the wave incidence angle for brick and concrete slabs bounded on both sides of air.

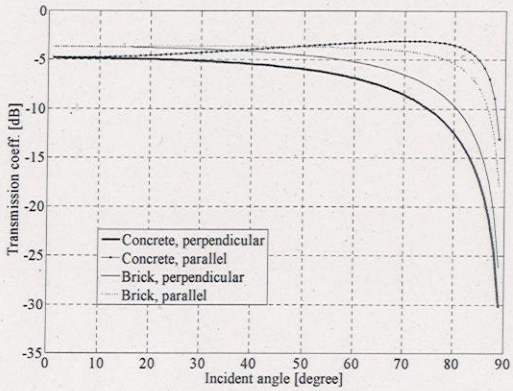

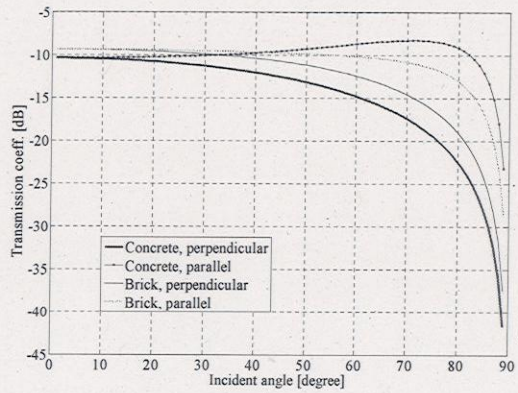

Figure 3 Transmission coefficient at 900 MHz Transmission coefficient at 2.4 GHz

The concrete and brick slab thicknesses are 12 cm with complex permittivity of ε_r = 9 -i*0.9 and ε_r = 2.8 -i*0.56 respectively.

The results are showing no significant difference in transmission coefficient for brick and concrete but this loss highly increase with frequency, therefore especially WLAN network areas notably limited by this factor in multiple wall indoor environment. (The reinforced concrete iron layer produces additional reflection and transmission loss which can be modeled using FDTD simulation)

The ray tracing method also uses the multiple layer transmission calculation but this simplification results in increasing error for short range radio environments where the material interfaces are in near field of the antennas or there are not by plane surfaces bounded. The FDTD method is able to model also the previous cases, even if there is excited by non sinusoidal time dependent source. The Figure 4 shows the field strength distribution for Gaussian pulse modulated sinusoidal excitation at different time with interaction of the wave by finite thickness lossy dielectric slab having permittivity of ε_r = 3-1*j. It is very obvious the wave decoupling into reflected and transmitted components.

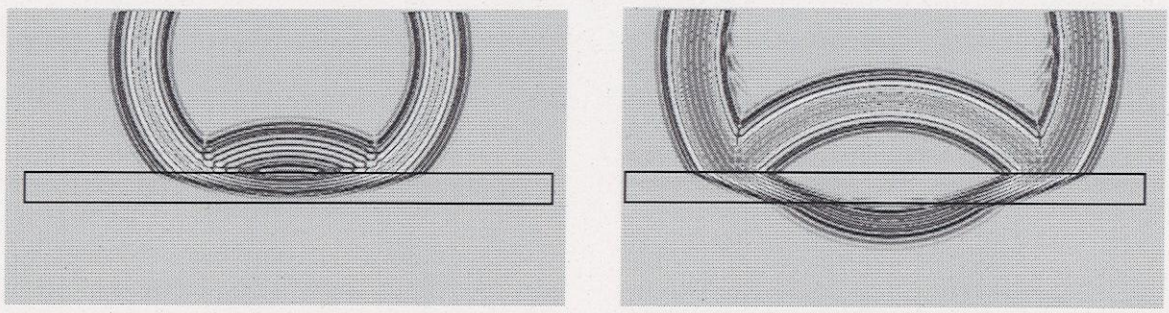

Figure 4 Wave transmission on finite thickness lossy dielectric excited by point source with $\perp$ polarization

2.4. Diffraction

Diffraction refers to the bending of waves around an edge of an object. Diffraction phenomenon depends on the size of the object relative to the wavelength of the wave. When the dimensions of the radiating object are large compared to the wavelength, high frequency asymptotic techniques can be used to analyze many otherwise not mathematically treatable problems. Basically the application of the diffraction theory was started in the area of physics which deals with the description of the light wave propagation.

The basic concept of geometrical optics, or ray optics is inadequate in many situations to completely describe the behavior of the electromagnetic field in the shadow region, behind the diffraction objects. The diffracted field is added to calculate the field contribution in the shadow region, and that permits us to solve many practical radio wave propagation problems.

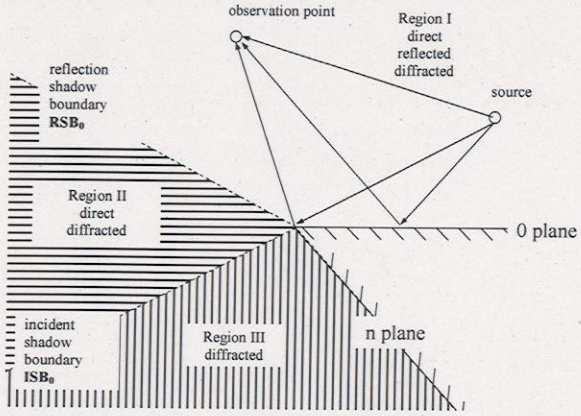

Figure 5/a Direct, reflection and diffraction regions

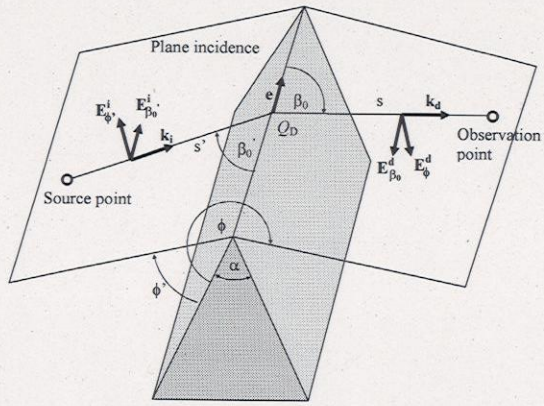

Figure 5/b Diffraction geometry

The diffraction components are expressed as

$$\begin{bmatrix} \mathbf{E}^d_{\beta_0}(s) \\ \mathbf{E}^d_{\phi}(s) \end{bmatrix} = -\begin{bmatrix} D_s & 0 \\ 0 & D_h \end{bmatrix} \begin{bmatrix} \mathbf{E}^i_{\beta_0'}(Q_D) \\ \mathbf{E}^i_{\phi'}(Q_D) \end{bmatrix} A(s',s)e^{-jks} \qquad (5)$$

where

$\mathbf{E}^i_{\beta_0'}(Q_D)$ the component of incident electrical field parallel to the plane of incidence at the point of diffraction, $\mathbf{E}^i_{\phi'}(Q_D)$ the component of incident electrical field perpendicular to the plane of incidence at the point of diffraction, D_S and D_h are the diffraction coefficients for soft and hard polarization.

$$A(s',s)=\begin{cases}\dfrac{1}{\sqrt{s\cdot\sin\beta_0}} & \text{for cylindrical incoming waves}\\ \sqrt{\dfrac{s'}{s(s+s')}} & \text{for spherical incoming waves}\end{cases}$$

The expression of diffraction coefficients are first derived by Keller publishing the Geometrical Theory of Diffraction (GTD). The GTD diffraction coefficients possess singularities along the incident and reflection shadow boundaries and therefore in the neighborhood of these boundaries the model is inapplicable.

In the later work of Kouyoumjian and Pathak removed the singularities by introducing the Uniform Theory of Diffraction (UTD) and in most wave propagation models this approach is used. The regions in the neighborhood of the shadows boundaries are referred to as transition regions, and these regions the fields undergo their most rapid changes. The diffraction coefficients are

$$D_h(\phi,\phi',n,\beta'_0)=\frac{e^{-j\pi/4}}{2n\sqrt{2\pi k}\sin\beta'_0}\left[D_0^{ISB}+D_n^{ISB}+R_0^h D_0^{RSB}+R_n^h D_n^{RSB}\right]$$
$$D_s(\phi,\phi',n,\beta'_0)=\frac{e^{-j\pi/4}}{2n\sqrt{2\pi k}\sin\beta'_0}\left[D_0^{ISB}+D_n^{ISB}+R_0^s D_0^{RSB}+R_n^s D_n^{RSB}\right] \qquad (6)$$

where $R_0^{h,s}$ and $R_n^{h,s}$ are the reflection coefficients on 0 and n planes represented in Figure 5/a, $D_{0,n}^{ISB,RSB}$ are the incident diffraction coefficient component at the Incident Shadow Boundary (ISB) and the reflected diffracted component at the Reflection Shadow Boundary (RSB) respectively.

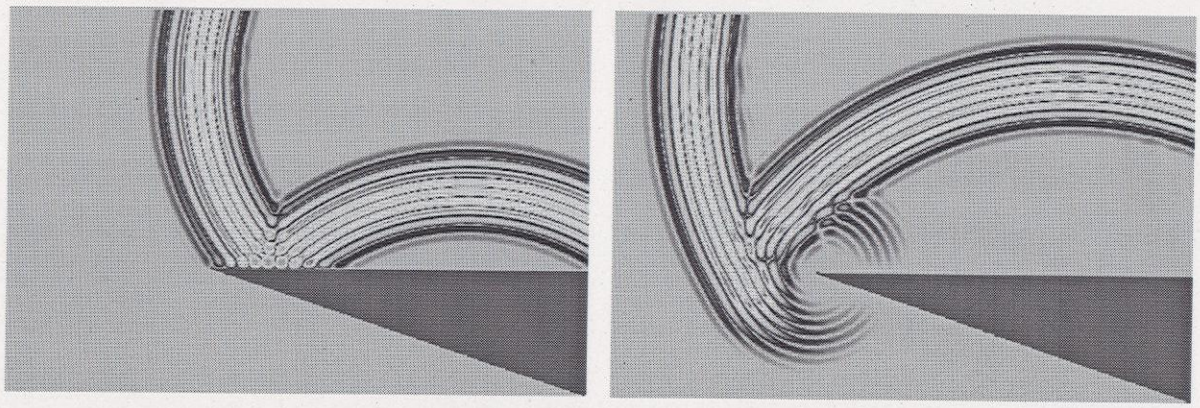

Figure 6 Diffraction on a lossy dielectric wedge

The Figure 6 shows a propagating wave before and after the diffraction on a lossy dielectric wedge for Gaussian modulated sinusoidal point source excitation and simulated by FDTD method.

3. Wave propagation models

To implement a mobile radio system, wave propagation models are necessary to determine propagation characteristics for signal and for interference powers any arbitrary installation and for any receiving positions. These models and results are the basis for the high-level network planning process.

The narrow band signals and simple building geometry make possible to apply empirical and semi-empirical models in the network design practice.

3.1. Deterministic models

Ray tracing

The ray tracing based radio wave propagation models are based on geometrical optics, instead of the entire domain field simulation. The method partitioning the propagation waves into finite angular components, and these propagation components are traced independently and applying to each the boundary conditions on material interfaces – reflection, transmission, diffraction. The solution on every observation points can be finally derived by summing the wave contributions.

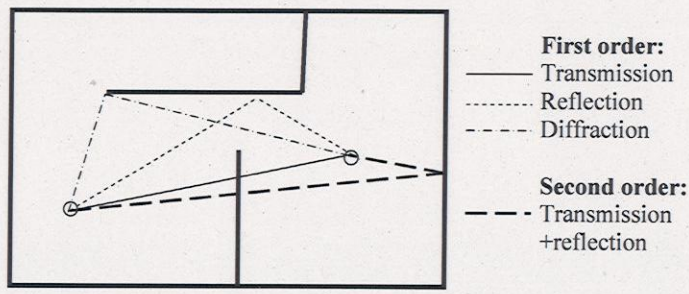

Figure 7 First and second order ray tracing components

The ray tracing method in practice uses either all possible first, second and third order combination of propagation mechanisms, or the ray components are traced till the field strength reaching a user defined threshold limit.

The Finite Difference Time Domain (FDTD) method

The FDTD method is a time domain solution of the Maxwell's equations described in differential form and is widely used in circuit analysis because of its simplicity. The method divide the space investigated into finite grid elements and on the grid the time and space approximation of the electrical and magnetic field strength is performed.

There exist many various forms of the FDTD in one, two or three dimensions and for many coordinate systems or grids and material types. For the indoor wireless channel simulation the three dimensional rectangular coordinate system was chosen with linear lossy dielectric materials in volumes.

Table 1 Ray tracing and FDTD method comparison

	Ray tracing	FDTD
Features	Frequency domain solution; Narrowband, harmonic excitation	Time domain solution; Broadband, arbitrary excitation
Advantages	The problem can be split into parts	Simple programming; Simple data base structure with volume elements;
Disadvantages	Difficulty in programming; In case of complex or rounded geometry the significant divergence of traced rays; Data base pre processing needed – the volume element have to be dissolve into boundary surface elements; Tremendous running time;	Tremendous running time and memory requirement

The method will be introduced briefly for general 3 dimensional case in rectangular coordinate system. Starting from the generalized differential matrix operators, the Maxwell's curl equations can be express in the rectangular coordinate system as

$$\frac{\partial E_x}{\partial t} = \frac{1}{\varepsilon}\left[\frac{\partial H_z}{\partial y} - \frac{\partial H_y}{\partial z} - \left(J_{source_x} + \sigma E_x\right)\right]$$

$$\frac{\partial E_y}{\partial t} = \frac{1}{\varepsilon}\left[\frac{\partial H_x}{\partial z} - \frac{\partial H_z}{\partial x} - \left(J_{source_y} + \sigma E_y\right)\right] \qquad (9)$$

$$\frac{\partial E_z}{\partial t} = \frac{1}{\varepsilon}\left[\frac{\partial H_y}{\partial x} - \frac{\partial H_x}{\partial y} - \left(J_{source_z} + \sigma E_z\right)\right]$$

Next the Yee algorithm is than used for a discrete grid and consider a substitution of central differences for the time ($\partial/\partial t$) and space ($\partial/\partial x$, $\partial/\partial y$, $\partial/\partial z$) derivatives in (9) one get for the time marching solution of the following coupled equations. The algorithm defines the six (E_x, E_y, E_z, H_x, H_y, H_z) discretized field components in the FDTD rectangular unit cell (the Yee cell). This cell has dimensions of $\Delta x \Delta y \Delta z$ and the electric and magnetic field components locations are interleaved by half of the discretization length ($\Delta x/2, \Delta y/2$ and Δz).

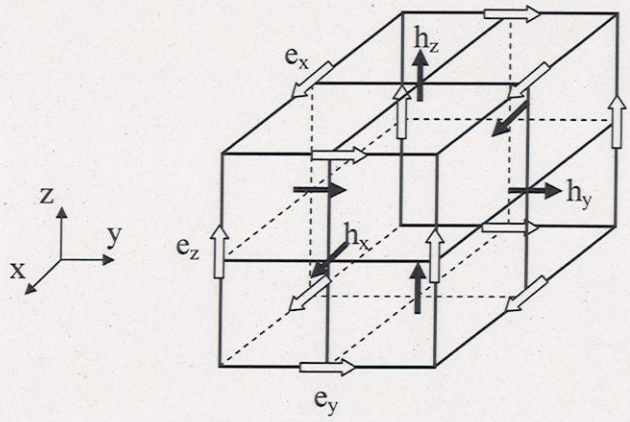

Figure 8 The 3 dimensional FDTD Yee cell with the electrical and magnetic reference vectors

In a similar manner calculating the fields every half-time step the centered difference for the time derivative is obtained.

The x directional electrical field strength component at the $n+1/2$ time step is

$$E_x\Big|_{i,j+1/2,k+1/2}^{n+1/2} = \left(\frac{1-\frac{\sigma_{i,j+1/2,k+1/2}\Delta t}{2\varepsilon_{i,j+1/2,k+1/2}}}{1+\frac{\sigma_{i,j+1/2,k+1/2}\Delta t}{2\varepsilon_{i,j+1/2,k+1/2}}}\right) E_x\Big|_{i,j+1/2,k+1/2}^{n-1/2} + \left(\frac{\frac{\Delta t}{\varepsilon_{i,j+1/2,k+1/2}}}{1+\frac{\sigma_{i,j+1/2,k+1/2}\Delta t}{2\varepsilon_{i,j+1/2,k+1/2}}}\right) \cdot \left(\begin{array}{l} \dfrac{H_z\Big|_{i,j+1,k+1/2}^{n} - H_z\Big|_{i,j,k+1/2}^{n}}{\Delta y} \\ -\dfrac{H_y\Big|_{i,j+1/2,k+1}^{n} - H_y\Big|_{i,j+1/2,k}^{n}}{\Delta z} \\ -J_{source_x}\Big|_{i,j+1/2,k+1/2}^{n} \end{array}\right)$$

(10)

Similar finite difference equations can be expressed for the other five field strength components, E_y, E_z, H_x, H_y and H_z.

The discretization on the simulation volume is made by cubic lattice so $\Delta x = \Delta y = \Delta z = \Delta$ which results in a significant simplification of the finite difference equations.

The $\varepsilon_{i,j,k}$ and $\sigma_{i,j,k}$ are the permittivity and conductivity of the material at the i,j,k discretisation position.

Stability of the FDTD solution requires that the electromagnetic wave must not pass through more than one cell in one time step, i.e., the time step and the unit cell dimension satisfy the Courant condition.

The Δt time step was chosen in accordance of this magic time step

$$\Delta t \leq \frac{1}{c\sqrt{\frac{1}{(\Delta x)^2}+\frac{1}{(\Delta y)^2}+\frac{1}{(\Delta z)^2}}} \tag{11}$$

which results $\Delta t \leq \frac{\Delta}{c\sqrt{3}}$ for our cubic lattice.

Special two dimensional geometries

The first investigation showed that the determination of field strength distribution in tunnel using full 3D model extends our calculation possibilities. Therefore we decided to model our geometry in two cut planes namely in the axial and in the radial plane. The two approximations differ basically because the axial cut plane can be applied in case of rotationally symmetric geometry and the radial plane is a cut of the tunnel waveguide which is assumed non changing cross section. (Figure 9)

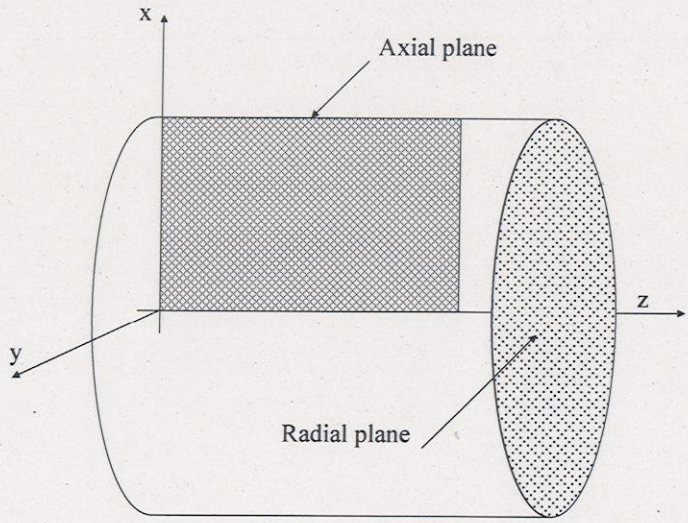

Figure 9 The axial and radial cut planes

Axial plane

Derivation of the cylindrical FDTD equations starting from the generalized differential matrix operators, the Maxwell's curl equations can be express in the cylindrical coordinate system as

$$\nabla \times \mathbf{E} = \begin{vmatrix} \mathbf{e}_r & \mathbf{e}_\varphi & \frac{1}{r}\mathbf{e}_z \\ \frac{\partial}{\partial r} r & \frac{\partial}{\partial \varphi} & \frac{\partial}{\partial z} \\ E_r & E_\varphi & \frac{1}{r}E_z \end{vmatrix} = -\frac{\partial \mu \mathbf{H}}{\partial t} + \sigma^m \mathbf{H} \tag{12}$$

$$\nabla \times \mathbf{H} = \begin{vmatrix} \mathbf{e}_r & \mathbf{e}_\varphi & \frac{1}{r}\mathbf{e}_z \\ \frac{\partial}{\partial r} r & \frac{\partial}{\partial \varphi} & \frac{\partial}{\partial z} \\ H_r & H_\varphi & \frac{1}{r}H_z \end{vmatrix} = \frac{\partial \varepsilon \mathbf{E}}{\partial t} + \sigma^e \mathbf{E} \tag{13}$$

where

ε is the permittivity,

μ is the permeability,

σ^e is the electric conductivity,

σ^m is the magnetic conductivity.

The φ variation of **E** and **H** in the cylindrical coordinates system will have the following form

$$\mathbf{E},\mathbf{H} = \sum_{m=0}^{\infty}\left[(\mathbf{e}_u,\mathbf{h}_u)\cos m\varphi + (\mathbf{e}_v,\mathbf{h}_v)\sin m\varphi\right] \tag{14}$$

where

m is the mode number.

Using the cylindrical symmetry of the geometry the 3D equations are reduced to 2D in the (x-z) r-z plane.

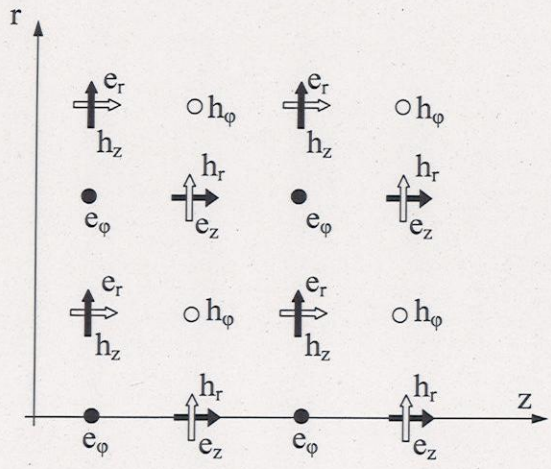

Figure 10 Electric and magnetic field components on the axial plane

After discretizing the Eq. 12-14, and applying the finite difference approximations to yield the updating equations for each field components.

$$E_r\big|_{i,k}^{n+1} = \left(\frac{1-\frac{\sigma_r^e\Delta t}{2\varepsilon_0\varepsilon_r}}{1+\frac{\sigma_r^e\Delta t}{2\varepsilon_0\varepsilon_r}}\right)E_r\big|_{i,k}^{n} - \left(\frac{\frac{\Delta t}{\varepsilon_0\varepsilon_r}}{1+\frac{\sigma_r^e\Delta t}{2\varepsilon_0\varepsilon_r}}\right)\left[\frac{H_\varphi\big|_{i,k}^{n+1/2} - H_\varphi\big|_{i,k-1}^{n+1/2}}{\Delta z} - \frac{m}{(i)\Delta r}H_z\big|_{i,k}^{n+1/2}\right] \tag{15}$$

$$E_\varphi\big|_{i,k}^{n+1} = \left(\frac{1-\frac{\sigma_\varphi^e\Delta t}{2\varepsilon_0\varepsilon_\varphi}}{1+\frac{\sigma_\varphi^e\Delta t}{2\varepsilon_0\varepsilon_\varphi}}\right)E_\varphi\big|_{i,k}^{n} + \left(\frac{\frac{\Delta t}{\varepsilon_0\varepsilon_\varphi}}{1+\frac{\sigma_\varphi^e\Delta t}{2\varepsilon_0\varepsilon_\varphi}}\right)\left(\frac{H_r\big|_{i,k}^{n+1/2} - H_r\big|_{i,k-1}^{n+1/2}}{\Delta z} - \frac{H_z\big|_{i,k}^{n+1/2} - H_z\big|_{i-1,k}^{n+1/2}}{\Delta r}\right) \tag{16}$$

where

$$i = r/\Delta r\,,\ k = z/\Delta z\,,\ n = t/\Delta t$$

Radial plane

The main steps will be introduced briefly for two-dimensional rectangular coordinate system. Starting from the generalized differential matrix operators, the Maxwell's equations can be express in the rectangular coordinate system as

For TM_z case

$$\frac{\partial E_z}{\partial t} = \frac{1}{\varepsilon}\left[\frac{\partial H_y}{\partial x} - \frac{\partial H_x}{\partial y} - J_{source_z}\right]$$

$$-\mu\frac{\partial H_x}{\partial t} = \frac{\partial E_z}{\partial y} \qquad (17)$$

$$-\mu\frac{\partial H_y}{\partial t} = \frac{\partial E_z}{\partial x}$$

For TE_z case similar expressions can be introduced.

Next the Yee algorithm is than used for a discrete grid and consider a substitution of central differences for the time and space derivatives in (17) one get for the time marching solution of the following coupled equations.

$$H_x\Big|_{j+1/2,k}^{n+1/2} = H_x\Big|_{j+1/2,k}^{n-1/2} - \frac{\Delta t}{\mu}\frac{E_z\Big|_{j+1/2,k+1/2}^{n} - E_z\Big|_{j+1/2,k-1/2}^{n}}{\Delta y} \qquad (18)$$

$$H_y\Big|_{j,k+1/2}^{n+1/2} = H_y\Big|_{j,k+1/2}^{n-1/2} + \frac{\Delta t}{\mu}\frac{E_z\Big|_{j+1/2,k+1/2}^{n} - E_z\Big|_{j-1/2,k+1/2}^{n}}{\Delta x} \qquad (19)$$

$$E_z\Big|_{j+1/2,k+1/2}^{n+1} = \frac{1-\xi}{1+\xi}E_z\Big|_{j+1/2,k+1/2}^{n} + \frac{1}{1+\xi}\frac{\Delta t}{\varepsilon}\frac{H_y\Big|_{j+1/2,k+1}^{n+1/2} - H_y\Big|_{j+1/2,k}^{n+1/2}}{\Delta x} - \frac{1}{1+\xi}\frac{\Delta t}{\varepsilon}\frac{H_x\Big|_{j+1/2,k+1}^{n+1/2} - H_x\Big|_{j+1/2,k}^{n+1/2}}{\Delta y} \qquad (20)$$

where

$$\xi = \frac{\sigma \Delta t}{2\varepsilon}$$

The discretization is made by cubic lattice on the simulation volume, and $\Delta x = \Delta y = \Delta$.

4. Results

4.1. Field strength distribution in the main two cut planes of tunnel

The application of the theory presented in Chapter 3 makes possible to investigate the mobile radio coverage in tunnels. The axial plane field strength distribution in a tunnel with radius 2 m at the distance of 1 m from the axis of symmetry for sinusoidal excitation source by frequency of 900 MHz. The results are in good agreement with analytical results of literature.

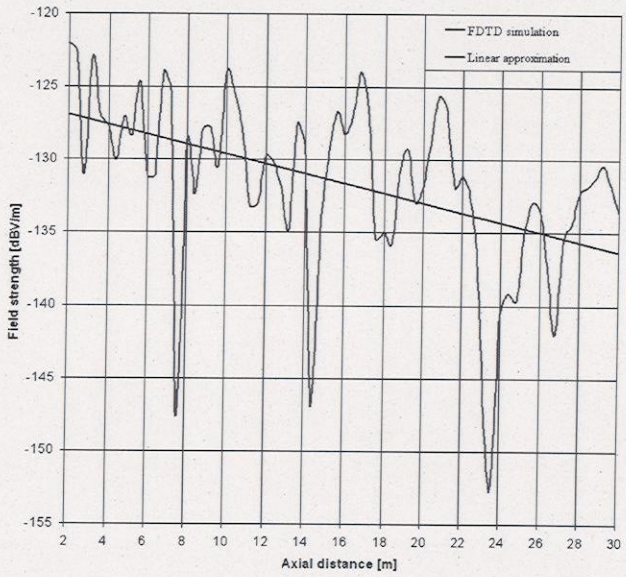

Figure 14 Electrical field strength vs. axial distance in tunnel

The gradient of the linear regression to the FDTD simulation results on Figure 14 is 9dB/decade which is indicating the waveguide nature of the tunnel at the frequency of investigation.

Our results in radial plane are showing the electric field strength distribution in the tunnel for point source sinusoidal time dependent excitation.

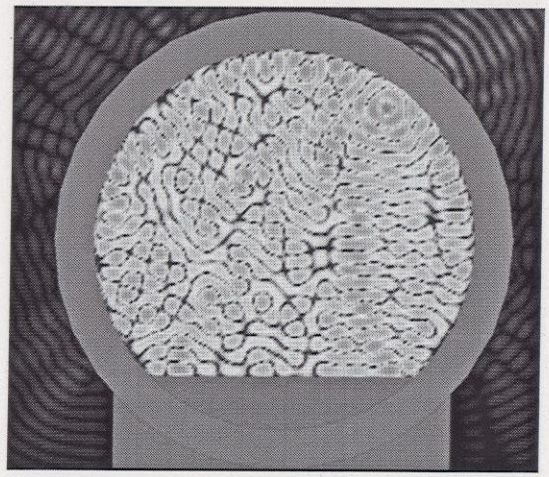

Figure 15 Field strength distribution of radial plane in tunnel

4.2. Path loss in axial plane of tunnel

Finally we summarize the path loss dependence along tunnel using different type of transmiter antennas.

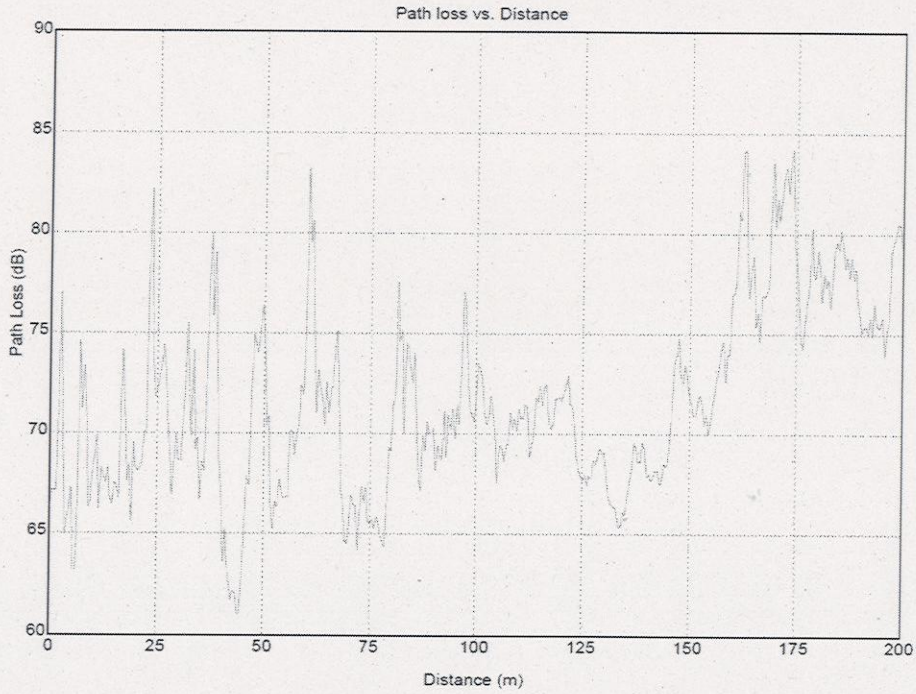

Figure 16 Path loss for dipole transmitter antenna, frequency 3GHz

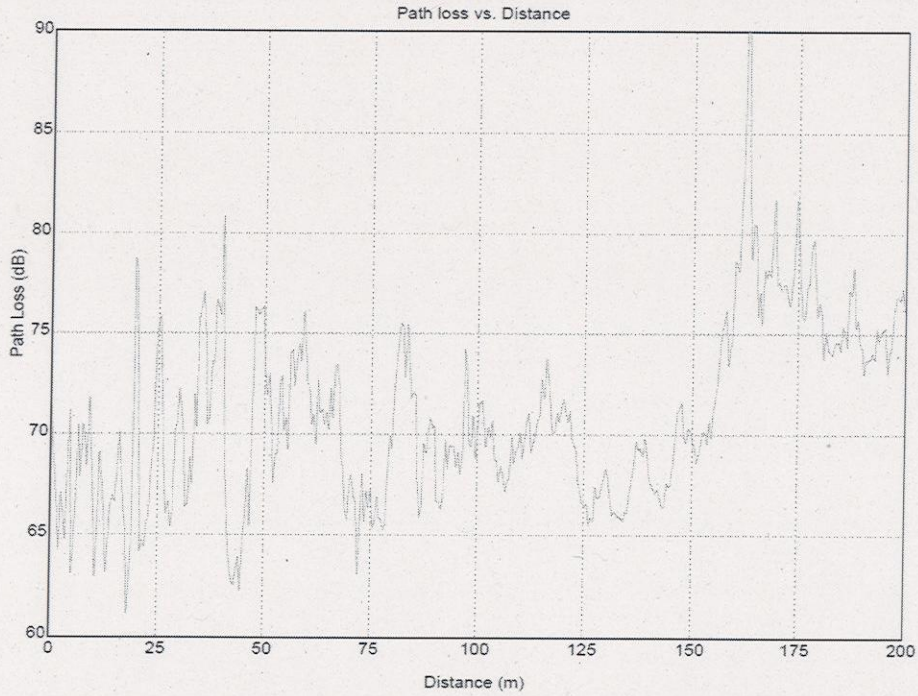

Figure 17 Path loss for horn antenna, 20x20cm aperture size, frequency 3GHz (45° beamwidth)

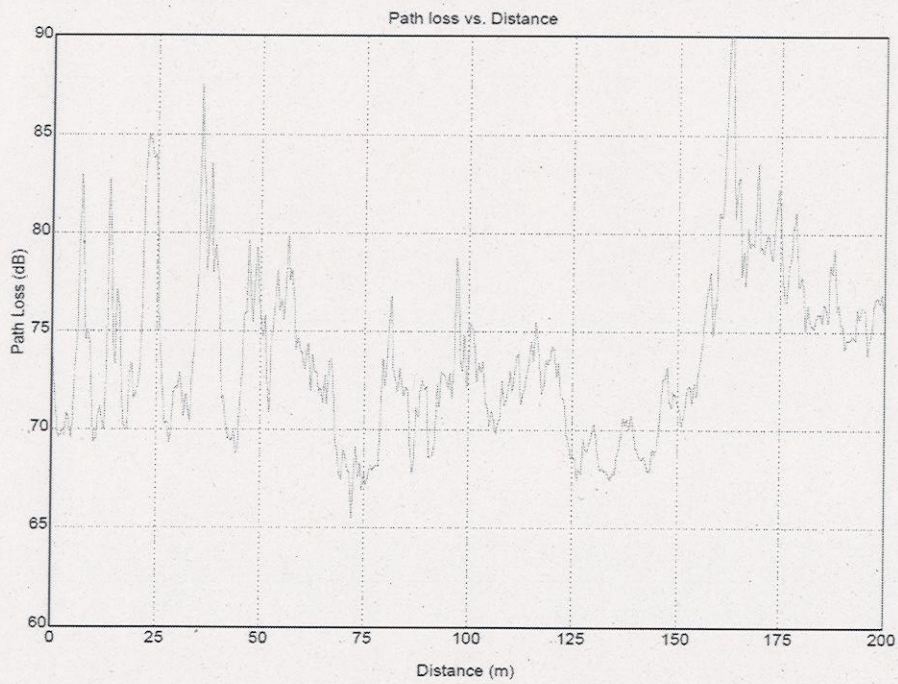

Figure 18 Path loss for horn antenna, frequency 3GHz (10° beamwidth)

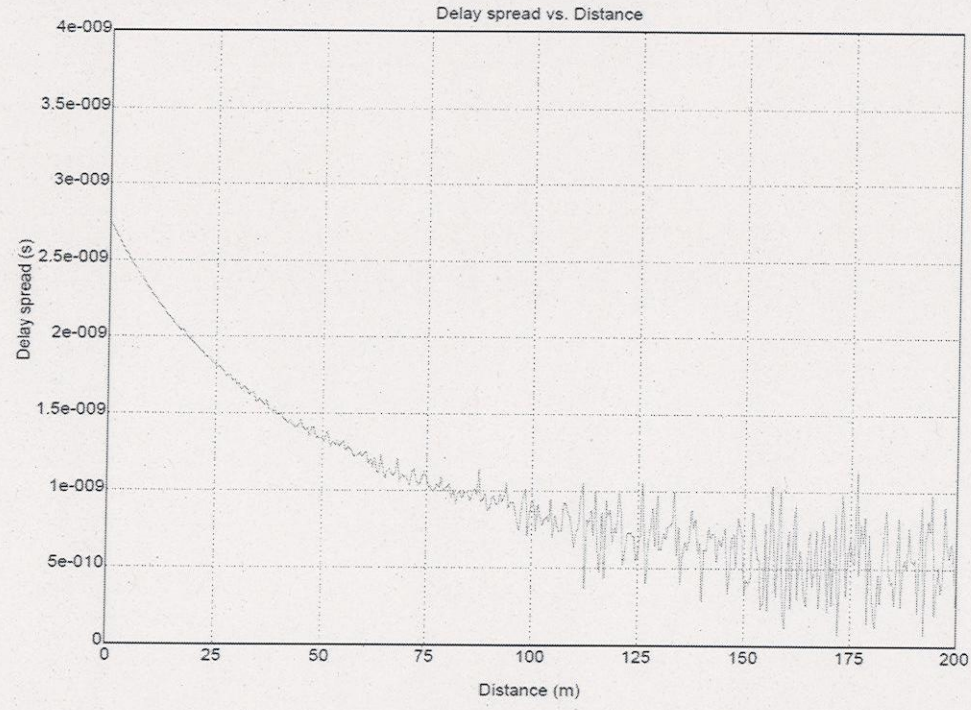

Figure 19 Delay spread for dipole transmitter antenna, frequency 3GHz

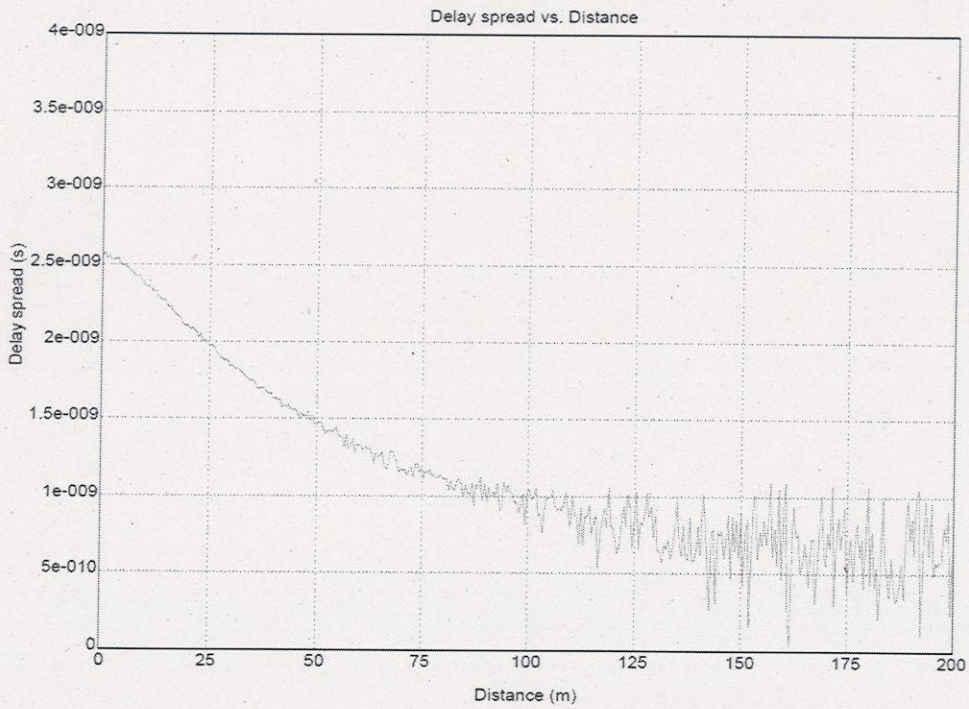

Figure 20 Delay spread for for horn antenna, 20x20cm aperture size, frequency 3GHz (45° beamwidth)

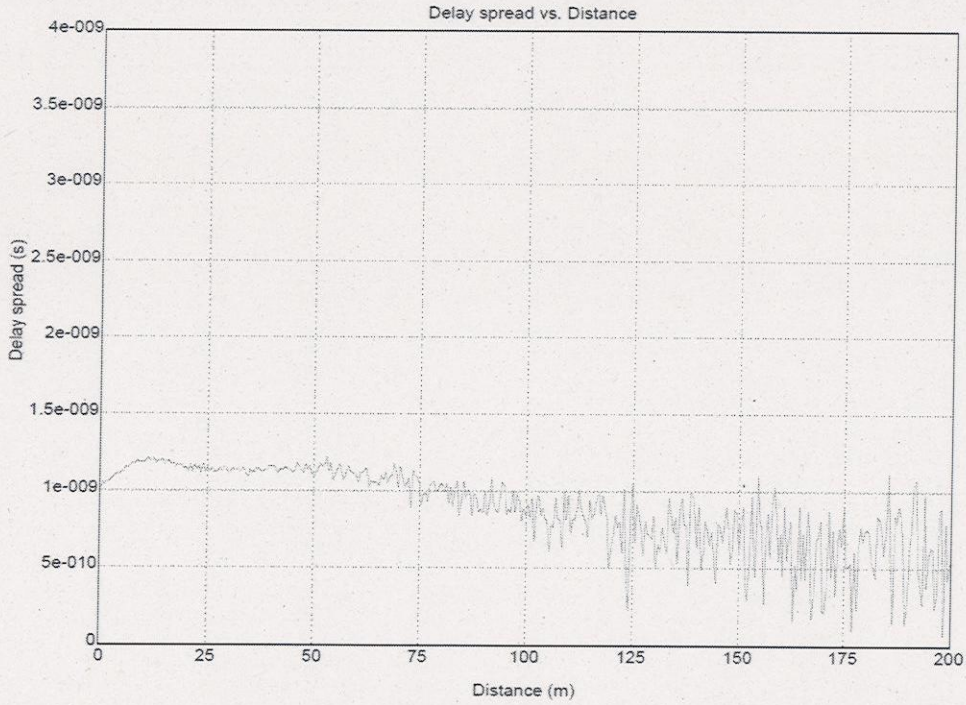

Figure 21 Delay spread for for horn antenna, frequency 3GHz (10^o beamwidth)

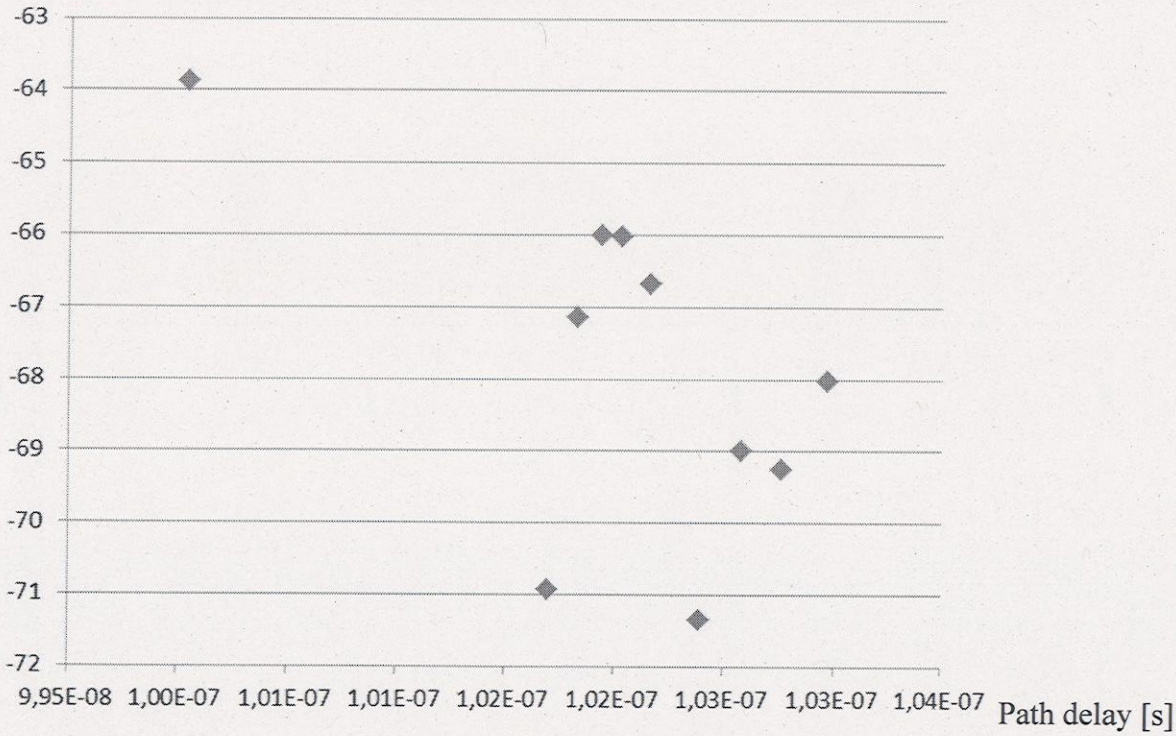

Figure 22 Path attenuations and delays for dipole transmitter antenna, frequency 3GHz

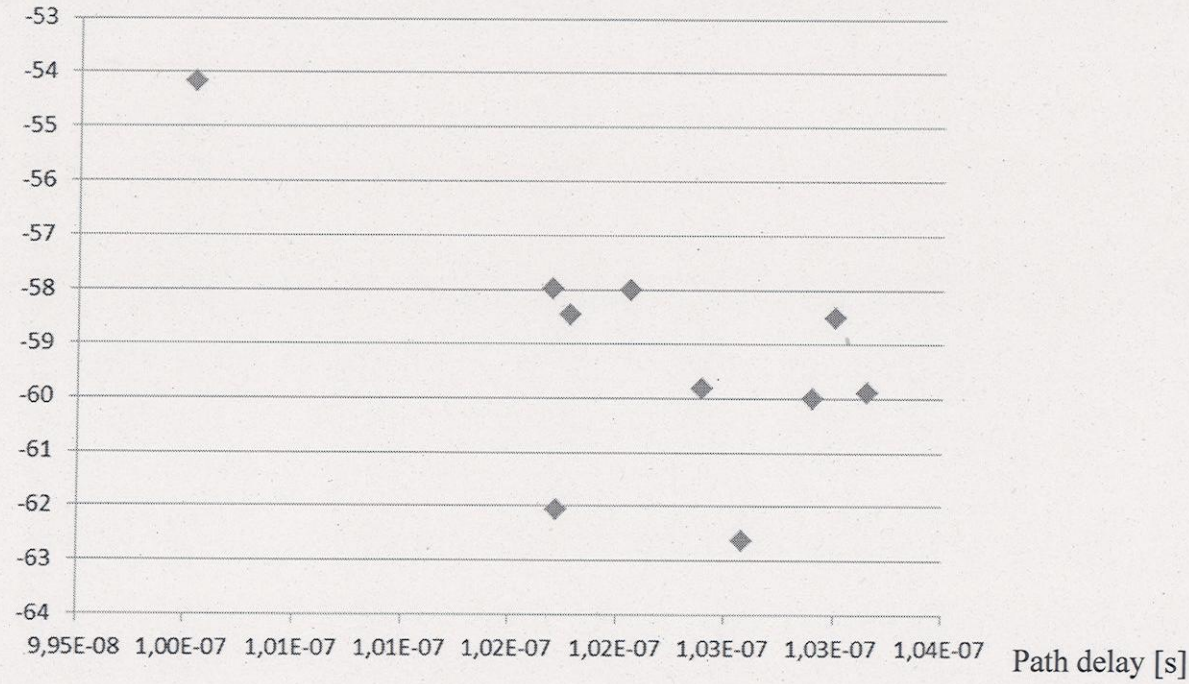

Figure 23 Path attenuations and delays for horn transmitter antenna, frequency 3GHz, (45° beamwidth)

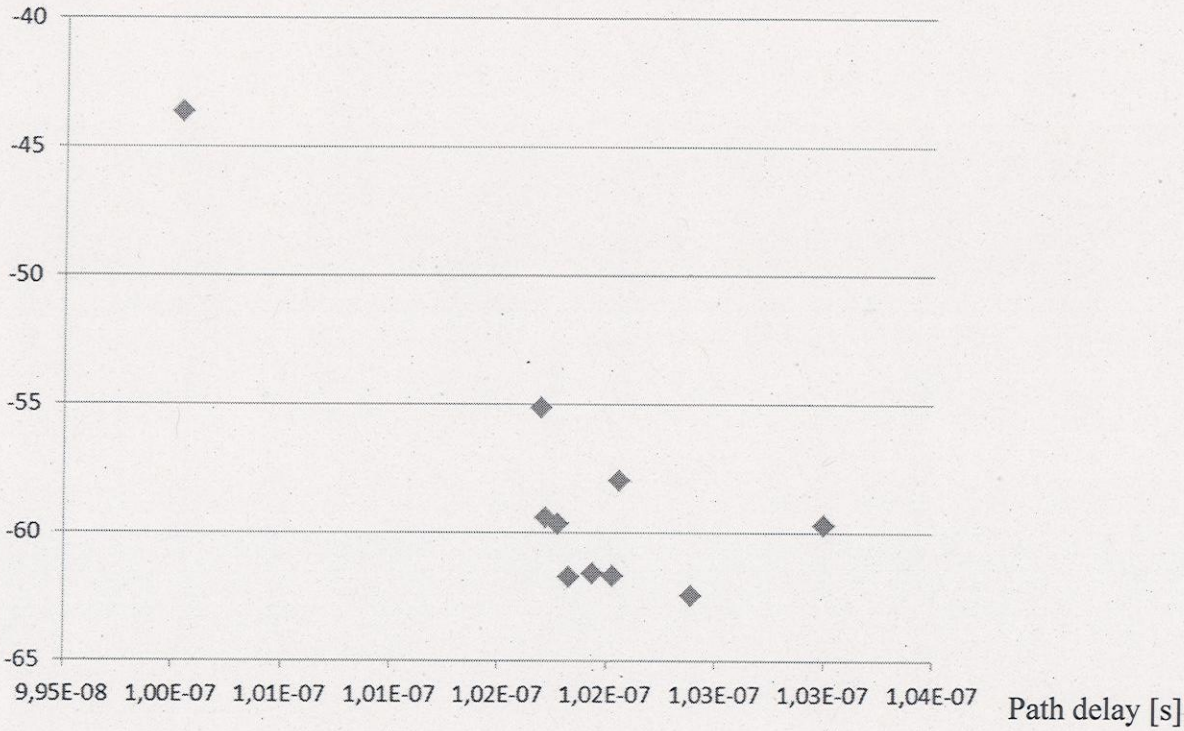

Figure 24 Path attenuations and delays for horn transmitter antenna, frequency 3GHz, (10° beamwidth)

5. Summary

Radio wave propagation attenuation in tunnels are presented and compared for applying different antennas as dipole and horn antennas.

The most important consequence can be derived from Figures 22-24. The delay spread can be significantly decreased using high gain transmitter antenna and each path component is below 10dB relative level for horn antenna of 10^{o} beamwidth.

References

[1] Lambertus J. W. van Loon, Mobile In-Home UHF Radio Propagation for Short-Range Devices, IEEE Antennas and Propagation Magazine, Vol. 41, No. 2, April 1999.

[2] Donald G. Dudley, Wireless Propagation in Circular Tunnels, IEEE Trans. Antennas Propagat., vol. 53, , pp. 435-441, 2005.

[3] Allen Taflove, Susan C. Hagness, Computational Electrodynamics: The finite-difference time-domain method, Artech House, Norwood, 2005

[4] V. Rodrigez-Pereyra, A.Z. Elsherbeni, C.E. Smith, A Body of Revolution Finite Difference Time Domain Method with Perfectly Matched Layer Absorbing Boundary, PIERS 24, pp. 257-277, 1999

[5] Yee, K. S., Numerical Solution of Initial Boundary Value Problems Involving Maxwell's Equations in Isotropic Media, IEEE Trans. Ant. Prop., 14(3), 302, 1966

[6] H. L. Bertoni, UHF Predictions for Wireless Personal Communications, Proceedings of the IEEE, 82, 9, 1994, p. 1333-1356.

[7] Constantine A. Balanis, Advanced Engineering Electromagnetics, John Wiley & Sons., 1989.

[8] Lajos Nagy, FDTD Field Strength Prediction for Mobile Microcells, ICECOM2005, 18th International Conference on Applied Electromagnetics and Communications, 12-14 October 2005, Dubrovnik, Croatioa,

[9] Lajos Nagy, MIMO cube in realistic indoor environment, The European Conference on Antennas and Propagation, EuCAP 2006, 6-10 November 2006, Nice, France

[10] Lajos Nagy, Propagation modeling in subway tunnel using FDTD, The European Conference on Antennas and Propagation, EuCAP 2006, 6-10 November 2006, Nice, France